CHAPTER SEVEN

Extending ITC to Kinetics with kinITC

Philippe Dumas*[,1], Eric Ennifar*, Cyrielle Da Veiga*, Guillaume Bec*, William Palau[†,‡], Carmelo Di Primo[†,‡], Angel Piñeiro[§,¶], Juan Sabin[§], Eva Muñoz[§], Javier Rial[§]

*Biophysics & Structural Biology Team, IBMC, UPR9002-CNRS, University of Strasbourg, Strasbourg, France
[†]University of Bordeaux, Laboratoire ARNA, Pessac, France
[‡]INSERM U869, Laboratoire ARNA, Pessac, France
[§]AFFINImeter Scientific & Development Team, Software 4 Science Developments, S. L. Ed. Emprendia, Campus Vida, Santiago de Compostela, A Coruña, Spain
[¶]Department of Applied Physics, Faculty of Physics, University of Santiago de Compostela, Campus Vida, Santiago de Compostela, A Coruña, Spain
[1]Corresponding author: e-mail address: p.dumas@ibmc-cnrs.unistra.fr

Contents

Abstract

Isothermal titration calorimetry (ITC) has long been used for kinetic studies in chemistry, but this remained confined to enzymatic studies in the biological field. In fact, the biological community has long had the tendency of ignoring the kinetic possibilities of ITC considering it solely as a thermodynamic technique, whereas surface plasmon resonance is seen as the kinetic technique *par excellence*. However, the primary signal recorded by ITC is a heat power which is directly related to the kinetics of the reaction. Here, it is shown how this kinetic signal can be recovered by using *kinITC*, the kinetic

Methods in Enzymology, Volume 567
ISSN 0076-6879
http://dx.doi.org/10.1016/bs.mie.2015.08.026

extension of ITC. The theoretical basis of *kinITC* is detailed for the most common situation of a second-order reaction $A + B \; \Omega \; C$ characterized by kinetic parameters k_{on}, k_{off}. A simplified *kinITC–ETC* method based upon the determination of an "Equilibration Time Curve" (ETC) is presented. The ETC is obtained by automatic determination of the "effective end" of each injection. The method is illustrated with experimental results with a comparison to Surface Plasmon Resonance (SPR) data. k_{on} values were obtained in a wide range, from 10^3 to 0.5×10^6 M^{-1} s^{-1}. All procedures were implemented in the program AFFINImeter (https://www.affinimeter.com/).

1. INTRODUCTION

Classical thermodynamics mentions time only when it comes to defining "reversible processes" that are necessary to evaluate state functions along the path of finite transformations. It is then imagined that the finite transformation takes place, in theory, infinitely slowly. This means that real kinetic considerations are in fact absent from classical thermodynamics. It is thus commonplace to view isothermal titration calorimetry (ITC) as the standard for thermodynamic studies by its ability to measure directly the enthalpy variation, but not as a technique from which can be derived kinetic information. Such a view is totally unjustified as the primary signal of ITC is a heat power in Joules per second (Watts), not the heat itself in Joules. It should be mentioned that this false view is more commonplace in biology than in chemistry where the link between the measured heat power and the kinetics of the reaction has long been investigated (Calvet & Prat, 1963; Garcia-Fuentes, Baron, & Mayorga, 1998; Lopez-Mayorga, Mateo, & Cortijo, 1987). Historically, this is somewhat strange as the first application of calorimetry by Lavoisier and Laplace was for measuring the heat power evolved by living animals. However, with studies on isolated biological processes (e.g., oxygen binding by hemoglobin) rather than on global physiological functions like respiration, an immediate limitation was that of the amount of biological material and the extreme smallness of the signal to be measured. This led to consider calorimetry as an almost inaccessible technique in biology, not even mentioning kinetic applications. These obvious facts explain why the usage of calorimetry remained for a long domain of pioneers in biology (Buzzell & Sturtevant, 1951; Langerman & Biltonen, 1979; Privalov, 1979; Tian & Cotie, 1924; Watt & Sturtevant, 1969; Wiseman, Williston, Brandts, & Lin, 1989) and why its introduction as a daily technique in biological labs lagged so much behind its usage in chemistry. Illustrative of this state of affair is the following statement by Edsall and

Gutfreund (1983), p. 210: "There are probably as many spectrophotometers […] in a single major university as there are calorimeters in all the biochemical laboratories in the world; but the number of calorimeters is sure to increase greatly in the next decade or two". However, even in chemistry, the large sample volumes and the long response times of the instruments, made that measurements remained limited to slow, and sometimes very slow reactions (Willson, Beezer, Mitchell, & Loh, 1995). A remarkable exception is the work by Johnson & Biltonen (1975). More recently (Hansen et al., 2010), kinetic measurements were performed on a textbook example of a very slow reaction lasting for 10 h (acid-catalyzed hydrolysis of sucrose) to illustrate the different methods of retrieving the kinetics of the reaction from the raw signal. This means that, even in chemistry, kinetic measurements by ITC do not seem to be widely spread.

It now appears that a new impetus is coming from biology after ITC has been rediscovered as a kinetic technique (Burnouf et al., 2012; Egawa, Tsuneshige, Suematsu, & Yonetani, 2007; Vander Meulen & Butcher, 2012). Such an emergence was obviously facilitated by the availability of modern instruments with cell volumes as small as 200 μL and response times of order of 3.5 s. However, in Vander Meulen and Butcher (2012), slow RNA folding could be studied efficiently with a VP-ITC (Microcal-Malvern) having a larger response time (ca. 10–12 s) (see Chapter "Measuring the kinetics of molecular association by isothermal titration calorimetry" by Vander Meulen et al., in this volume). One can thus anticipate that *kinITC*, as it was coined in Burnouf et al. (2012), has the potentiality of becoming a standard kinetic technique in biology.

We showed in a previous work that, not only simple reactions like $A + B \leftrightharpoons C$ but also more complex reactions involving a two-step kinetic mechanism (e.g., "induced-fit mechanism"), could be addressed by *kinITC* (Burnouf et al., 2012). In this chapter, we will focus exclusively on simple bimolecular reactions and, particularly, on the analysis of a simplified *kinITC* method that was recently introduced in the program AFFINImeter (S4SD, Santiago de Compostela, Spain; https://www.affinimeter.com/). We called this simplified method *kinITC–ETC* as it is based upon the determination of the effective end of each injection which yields an "Equilibration Time Curve", in short *ETC*, allowing to retrieve the kinetic parameters k_{on}, k_{off}. We will first present the theoretical basis of *kinITC–ETC* and the limitations that may be anticipated. The method will be illustrated by three experimental examples for which SPR measurements are available: (1) interaction of HIV-1 Reverse Transcriptase (RT) with its inhibitor

Nevirapine, (2) interaction of carbonic anhydrase with its inhibitor 4-carboxybenzenesulfonamide (4-CBS), (3) interaction of two complementary DNA strands. Cases (1) and (3) not only provided reasonable results but also allowed illustrating the problems occurring for opposite reasons, respectively, very slow association ($k_{on} \sim 1500\ M^{-1}\ s^{-1}$) being the cause of poor affinity and too fast association ($k_{on} \sim 10^6\ M^{-1}\ s^{-1}$ above 32 °C). Case (2) is illustrative of a typical favorable situation at all temperatures.

2. THE THEORETICAL BASIS OF *kinITC–ETC*

The basis of *kinITC* only requires textbook considerations on chemical kinetics. In simple situations corresponding to a bimolecular reaction:

$$A + B \leftrightharpoons C \quad \text{with parameters } k_{on}, k_{off} \tag{1}$$

The kinetics of the reaction is represented by the differential equation:

$$\frac{d[C]}{dt} = k_{on}[A][B] - k_{off}[C] \tag{2a}$$

We will immediately transform it by using the reduced concentrations $A = [A]/[A]_{tot}$, $B = [B]/[A]_{tot}$, and $C = [C]/[A]_{tot}$, $[A]_{tot}$ being the total concentration of the titrand in the measurement cell:

$$\frac{dC}{dt} = k_{on}[A]_{tot}AB - k_{off}C \tag{2b}$$

This allows manipulating molar fractions that have a clear meaning, rather than absolute concentrations. The terms A, B, C, therefore, represent dimensionless "concentrations" when not used explicitly as "compound A, B, or C." In the following, it is assumed that compound B is in the syringe. Equation (2b) represents perfectly the kinetics of the reaction at any step of a titration, that is at any injection, if one considers the evolution of the concentrations after compound B has been injected (to be rigorous, the injection time should be increased slightly to take into account the mixing time). For this simplified *kinITC* method (but not in the full *kinITC* method), the small concentration variations resulting from the course of the reaction during the injection period are neglected, but the concentration variations due to dilution are not.

By using conservation equations $[A] + [C] = [A]_{tot}$ and $[B] + [C] = [B]_{tot}$, where $[A]_{tot}$ and $[B]_{tot}$ are, respectively, the total concentrations of

compounds A and B after injection, one is led by classical methods (see Burnouf et al., 2012; Dumas, 2015) to:

$$\frac{\mathrm{d}C}{\mathrm{d}t} = k_{\mathrm{on}}[A]_{\mathrm{tot}}(C - C_1)(C - C_2) \tag{3a}$$

C_1 and C_2 being the roots of $k_{\mathrm{on}}[A]_{\mathrm{tot}}(1 - C)(s - C) - k_{\mathrm{off}}C = 0$ (with $C_1 > C_2$):

$$C_1 = \frac{1}{2}\left(p + \sqrt{p^2 - 4s}\right), \quad C_2 = \frac{1}{2}\left(p - \sqrt{p^2 - 4s}\right); \quad p = 1 + s + \frac{K_{\mathrm{d}}}{[A]_{\mathrm{tot}}} \tag{3b}$$

with $s = [B]_{\mathrm{tot}}/[A]_{\mathrm{tot}}$ being the stoichiometric ratio for the current injection and $K_{\mathrm{d}} = k_{\mathrm{off}}/k_{\mathrm{on}}$ the dissociation constant. Again, note that $[A]_{\mathrm{tot}}$ varies from injection to injection due to the dilution resulting from injection of compound B.

Interestingly, the difference $(C_1 - C_2)$ is equal to $\widetilde{A} + \widetilde{B} + c^{-1}$ where $\widetilde{A}, \widetilde{B}$ are the reduced equilibrium concentrations (i.e., divided by $[A]_{\mathrm{tot}}$) of, respectively, compounds A and B, and $c = [A]_{\mathrm{tot}}/K_{\mathrm{d}}$ is the Wiseman parameter (Wiseman et al., 1989). By integration of the differential Eq. (3a) following standard methods, it is obtained:

$$C(t) = C_1 - \frac{C_1 - C_2}{1 - K^{-1}\mathrm{e}^{-t/\tau}}; \quad K^{-1} = \frac{C_2 - C_0}{C_1 - C_0} \tag{4a}$$

$$\tau^{-1} = k_{\mathrm{on}}[A]_{\mathrm{tot}}(C_1 - C_2) = k_{\mathrm{on}}[A]_{\mathrm{tot}}\left[\left(1 + c^{-1} + s\right)^2 - 4s\right] \tag{4b}$$

with $C_0 = C(t = 0)$ for the current injection and τ a characteristic time of the evolution of concentrations. From Eq. (4a), the following approximation $C(t) \approx C_2 - (C_1 - C_2)K^{-1}\mathrm{e}^{-t/\tau}$ holds for sufficiently large values of t/τ, which means that τ is representative of a single exponential, but only for sufficiently large values of t/τ. In order to make use of a quick and simplified *kinITC* method based upon the determination of the time necessary to return to baseline, it is important to evaluate how the effective characteristic time evolves during the equilibration process, particularly close to the end of the equilibration process. This is performed in the following.

It can be shown (Dumas, 2015) that $C(t)$ can be expressed rigorously as:

$$C(t) = C_1 - (C_1 - C_2)\sum_{n=0}^{n=\infty} K^{-n}\mathrm{e}^{-nt/\tau} \tag{5}$$

and since the heat power evolved during the reaction is $P_s(t) = V_{cell}\ \Delta H\ [A]_{tot} dC/dt$, by considering the expression for τ (Eq. 4b), it is obtained:

$$P_s(t) = V_{cell} \Delta H k_{on} [A]_{tot}^2 (C_1 - C_2)^2 \sum_{n=1}^{n=\infty} n K^{-n} e^{-nt/\tau} \quad (6)$$

This corresponds to the instantaneous heat power evolved in the measurement cell, and not to the actually measured heat power $P_m(t)$ due to the finite response time τ_{ITC} of the instrument. Taking this into account leads to (Dumas, 2015):

$$P_m(t) = V_{cell} \Delta H\ k_{on} [A]_{tot}^2 (C_1 - C_2)^2 \sum_{n=1}^{n=\infty} n K^{-n} \frac{e^{-nt/\tau} - e^{-t/\tau_{ITC}}}{1 - n\tau_{ITC}/\tau} \quad (7)$$

Admittedly, invoking a single time to characterize the response of an instrument may be a simplification (Garcia-Fuentes et al., 1998; Lopez-Mayorga et al., 1987; Tachoire, Macqueron, & Torra, 1986). However, with our instrument (ITC200 from Malvern-Microcal), we have observed that this is quite a reasonable assumption (see Section 5). We do not claim that all instruments behave exactly in the same way.

It is of interest that the comparison of Eqs. (6) and (7) shows directly the influence of the instrument response time on each component of the infinite sum through the replacement of $e^{-nt/\tau}$ with $\left(e^{-nt/\tau} - e^{-t/\tau_{ITC}}\right)/(1 - n\tau_{ITC}/\tau)$. It can be shown that $K^{-1} < 1$ and it follows that the successive terms in Eq. (7) become less and less important and, practically, a finite number of terms is sufficient (Fig. 1). Note that at the scale of the figure, at most five components among seven are visible.

After a detailed examination (Dumas, 2015), it was shown that, in most occasions, the first component alone governs the return to baseline of $P_m(t)$ after sufficient time following injection (ca. $t > 2\tau$, with τ being determined by Eq. 4b). This means that locating the effective end time of an injection, i.e., the time after which $P_m(t)$ may be considered as null, provides direct information on the time τ and thus on the kinetic parameters. The simplified *kinITC* method, therefore, is based upon the determination of the effective end time or, in other words, of the equilibration time of each injection, which yields a more or less bell-shaped ETC. Examples of such ETCs are in Figs. 4, 6, and 9. All links of the geometric features of an ETC to few relevant parameters are given in Appendix.

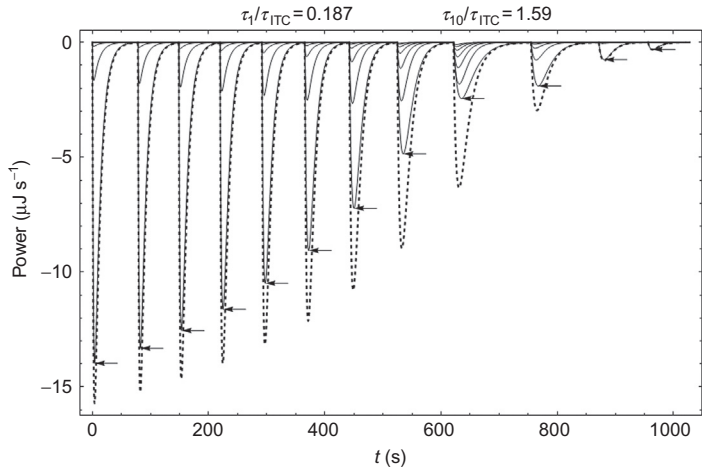

Figure 1 Illustration of the successive components in Eq. (7). The components from $n = 1$ to $n = 7$ in Eq. (7) are superimposed (thin curves). The max amplitude of each first component is indicated by an arrow. The sum of all components corresponds to the measured signal (dashed curve). The simulation was performed with the values: cell volume = 1.4 mL, injected volume at each injection = 12 μL, $[A]_0 = 20\ \mu M$ (cell), $[B]_0 = 240\ \mu M$ (syringe), $k_{on} = 3 \times 10^4\ M^{-1}\ s^{-1}$, $k_{off} = 10^{-3}\ s^{-1}$, $\Delta H = -80$ kJ mol^{-1}, $\tau_{ITC} = 10$ s. The term τ_1 and τ_{10} corresponds, respectively, to the characteristic times defined in Eq. (4b) for injections #1 and #10 (unit stoichiometry).

3. PRACTICAL ASPECTS OF THE METHOD

3.1 ETC Determination in Practice

The necessary methods (automatic baseline determination, integration of the injection power curves and ETC determination) allow determining automatically the "effective end" of each injection and the result matches closely what would have been obtained "by eye" (arrows in Fig. 2). It is obvious from inspection of Fig. 2 that the uncertainty on the equilibration time depends essentially on the signal/noise ratio of the base line.

3.2 Determination of k_{on} and k_{off} from the ETC

Once the ETC has been determined, a link has to be made between the "effective end time" $t_{end}(N_{inj})$ determined at injection $\#N_{inj}$ to the time $\tau(N_{inj})$ defined by Eq. (4b). The following approximation is used:

$$t_{end}\left(N_{inj}\right) = \alpha\left[\tau\left(N_{inj}\right) + \tau_{ITC}\right] + \tau_{inj} + \tau_{mix} \tag{8}$$

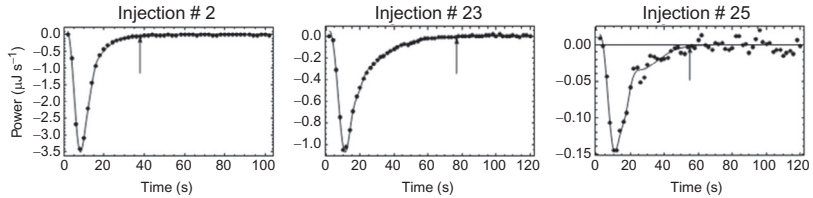

Figure 2 Determination of the "effective end" of each injection $P_m(t)$. Three particular injections of a titration of the oligoDNA 5′-AAG AAG AGG AG-3′ with its complementary strand are shown. The arrows mark the automatically determined "effective end" of each injection. Injection #23 corresponds to the injection with the longest equilibration time. Experimental conditions: $[A]_0 = 11.6\,\mu M$, $[B]_0 = 100\,\mu M$, injections of 1 µL, cell volume = 203.6 µL, sampling time = 2 s.

where α was tuned to 4.5 after trials and errors and τ_{inj} and τ_{mix} are, respectively, the injection time and the mixing time. Normally, there is a rule given by the manufacturer for the injection time (e.g., 2 s/µL injected with the ITC200 from Microcal-Malvern). The mixing time (of the order of 1 s) corresponds to the characteristic time of the exponential governing the approach to complete mixing of compound B after its injection in the cell. For the complete *kinITC* method with the aim of simulating exactly, the whole injections, τ_{inj} and τ_{mix}, have an important influence during, and immediately after, the injection (see realistic simulations on our web site at http://www-ibmc.u-strasbg.fr:8080/webMathematica/kinITCdemo/); for the simplified *kinITC-ETC* method, these two parameters are solely involved in the approximate correction to $t_{end}(N_{inj})$ by Eq. (8).

Importantly, if τ_{inj}, τ_{mix}, and τ_{ITC} are known, only k_{on} is unknown in the fit of an experimental ETC with Eqs. (4b) and (8), since $c = [A]_{tot}/K_d$ is known from the usual processing of the titration curve and since, obviously, the stoichiometric ratio s is known at each injection. In fact, even though τ_{ITC} can be determined experimentally (see below), it appeared that an efficient pragmatic solution was (most often) to consider τ_{ITC} as a free parameter too (Dumas, 2015). There are several reasons for this choice. First, τ_{ITC} may not be known accurately if it was measured too early before the experiment. Second, the conditions used for the determination of τ_{ITC} may not be exactly relevant for the conditions of the experiment (in particular, due to differences in the viscosity and the heat conductivity of the solution). Third, Eq. (8) is only approximate and, for this reason, it may be necessary to adjust τ_{ITC}.

4. RESULTS

4.1 Results with Carbonic Anhydrase and Its Inhibitor 4-CBS

Carbonic anhydrase is a zinc-containing enzyme that interconverts H^+ and bicarbonate HCO_3^- to CO_2 and water. As such, it has an essential role in pH regulation and respiration. This was an obvious choice as it was used in an extensive SPR benchmark involving 22 laboratories (Navratilova et al., 2007). In this way, the best possible kinetic parameters were available for comparison with the results from *kinITC–ETC*. The enzyme (bovine carbonic anhydrase II from Sigma Chemical), inhibitor 4-CBS (Acros Organics), and the buffer conditions used for ITC were identical to those used for the SPR study. Protein and ligand concentrations as well as the temperatures used are in the legend of Fig. 4. Baseline-corrected data are shown for two temperatures in Fig. 3 and the experimental ETCs with their fits with Eqs. (4b) and (8) are shown in Fig. 4. Since different temperatures were used in both types of experiments, the results are presented in the form of Arrhenius plots (Fig. 5).

Although the results are noisier for *kinITC-ETC*, the straight lines from the fit of $\ln(k_{on/off})$ versus T^{-1} are parallel within experimental errors, which points to identical activation energies and, thus, identical temperature dependence of k_{on} and k_{off} from the two methods. The straight lines from *kinITC-ETC* are systematically lower than those from SPR but at most by 0.5, which corresponds to $k_{on}(\mathrm{SPR})/k_{on}(\mathrm{kinITC-ETC}) \approx k_{off}(\mathrm{SPR})/k_{off}(\mathrm{kinITC-ETC}) \leq 1.65$ in the temperature range common to the two types of experiments (6.1–25 °C). Notably, this ratio was significantly higher (ca. 2.5) when τ_{ITC} was not considered as a free parameter and

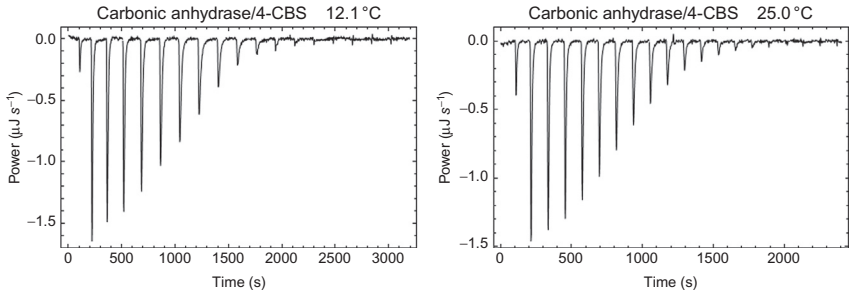

Figure 3 Example of baseline-corrected injection curves for carbonic anhydrase/4-CBS.

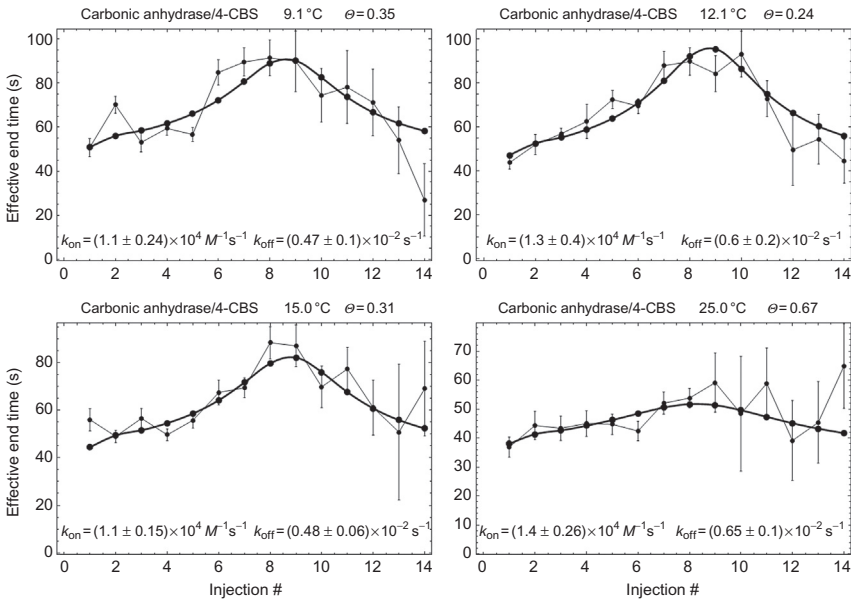

Figure 4 Fit of carbonic anhydrase ETCs at various temperatures. The initial concentrations of carbonic anhydrase (compound *A*) were $[A]_0 = 24.4$, 24.2, 24.5, 24.6, and 17.6 μ*M* at, respectively, 6.1 °C (not shown), 9.1, 12.1, 15, and 25 °C. The concentration of 4-CBS was $[B]_0 = 315\,\mu M$ at all temperatures and the injected volumes were 1.9 μL up to 15 °C and 1.4 μL at 25 °C. The parameter Θ indicated on top of each figure is defined in Table 1 and discussed in Appendix.

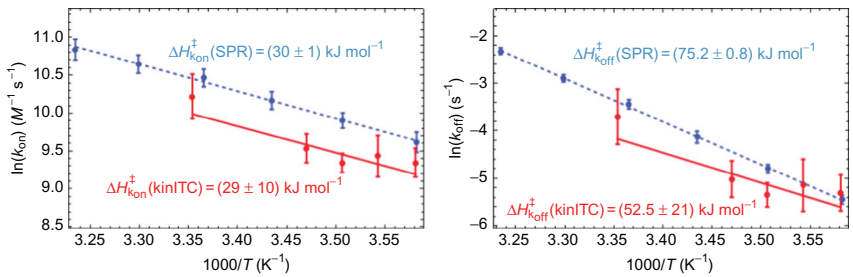

Figure 5 Arrhenius plots for the comparison of *kinITC–ETC* and SPR results. The *kinITC–ETC* results (continuous lines) are compared to the SPR results (dashed lines). The corresponding activation energies are indicated.

fixed to 3.5 s (not shown). This experimental case, therefore, appears to be representative of a favorable situation leading to kinetic parameters comparing well with those from SPR results of the best possible quality due to the unusually great number of independent replicate experiments.

4.2 Results with HIV-1 RT and Its Inhibitor Nevirapine

HIV-1 RT is a key enzyme in the life cycle of the virus and Nevirapine was the first discovered nonnucleoside inhibitor (De Clercq, 1998). This is a hydrophobic compound which is deeply buried within the protein. Interestingly, the binding site revealed by X-ray crystallography (PDB: 1VRT) is not preformed (Ren et al., 1995), which means that the ligand has to select transient favorable conformations to "find its way." We already used RT/nevirapine in the work for the original *kinITC* method for which we also had kinetic measurements by SPR (Burnouf et al., 2012). Three temperatures (25, 30, and 35 °C) were used for the ITC experiments, but SPR was performed only at 25 °C. Due to the hydrophobic character and limited solubility of Nevirapine, RT was used as compound *B* in the syringe to avoid using Nevirapine at too high concentrations. Here, we simply reprocessed the ITC data by *kinITC–ETC* (Fig. 6). Comparison of the results obtained here by *kinITC–ETC*, and by *kinITC* and SPR in Burnouf et al. (2012) is shown in Fig. 7. Recall that the results obtained by the full *kinITC* method are equations that can be plotted as continuous curves.

Overall, the different results are compatible with the largest discrepancy being a factor of three between *kinITC–ETC* and *kinITC*/SPR for k_{off} at 25 °C. Notably, the replicates of the SPR experiments also differed by a factor of two for k_{on}. Nevertheless, these results are all in agreement with the expected slow binding due to the necessary conformational change of the protein to accommodate the ligand. This interpretation is also in line with

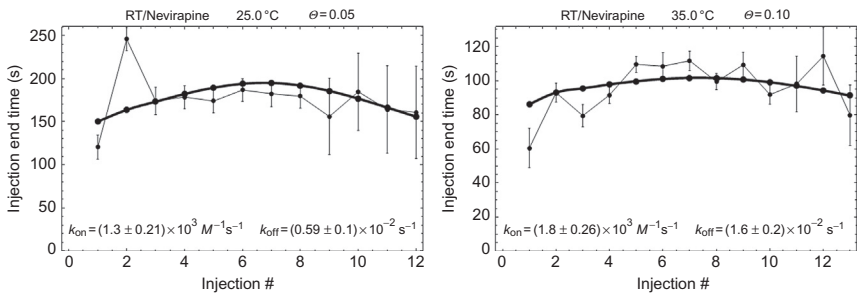

Figure 6 Fit of RT/Nevirapine ETCs. The initial concentrations were 20 μ*M* for nevirapine (compound *A*), 240 μ*M* for RT and the injected volumes were 2.33 μL. The different temperatures were 25, 30 (not shown), and 35 °C. Notably, the response time was kept fixed to 3.5 s as considering it as a free parameter in the fit led to aberrant negative values at 30 and 35 °C. The parameter Θ indicated on top of each figure is defined in Table 1 and discussed in Appendix.

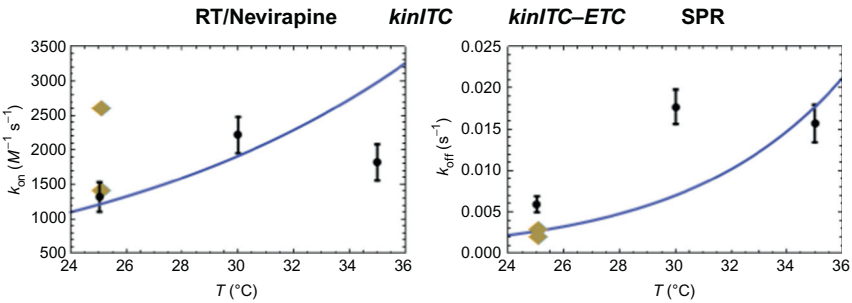

Figure 7 Comparison of *kinITC*, *kinITC–ETC*, and SPR results for RT/Nevirapine. The *kinITC* results from Burnouf et al. (2012) (solid line) and *kinITC-ETC* results (dots with error bar) are compared to the SPR results (diamonds).

the unfavorable large negative value of $\Delta S(\text{binding}) = -145$ J mol^{-1} K^{-1} at 25 °C (Burnouf et al., 2012), which marks an important stabilization of the protein upon ligand binding.

These results also show that very slow binding is not synonymous with great accuracy in *kinITC-ETC*. In fact, this slow binding implies a rather low affinity ($K_d = 4.4$ μM at 25 °C and 8.6 μM at 35 °C) which leads to very low c values (4.9 at 25 °C and 3.2 at 35 °C). In agreement with the theoretical results (Lines 2 and 3 of Table 1 in Appendix), the relative variation of the equilibration time is at most 20% and the characteristic bell shape of the ETC appears little due to the errors on the determination of the equilibration times (Fig. 6). The greatest part of the information, therefore, lies in the large equilibration time (well above $4.5\,\tau_{ITC}$) right from the first injections.

4.3 Results with the Annealing of Two Complementary DNA Strands

In order to test *kinITC-ETC* with fast association rates, we studied duplex formation from the polypurine DNA oligomer ODN$_1$ = 5′-AAG AAG AGG AG-3′ and its complementary sequence ODN$_2$. It has long been established that duplex formation from two DNA strands proceeds through two consecutive kinetic steps: initial formation of an unstable nucleus of three base pair followed by a "zipping" process leading to full duplex (Craig, Crothers, & Doty, 1971; Porschke & Eigen, 1971). However, according to these land-mark studies, the overall process can nevertheless be accurately described kinetically by a "global" single-step mechanism

$S_1 + S_2 \leftrightharpoons D$, because the zipping process is extremely fast in comparison of the formation of the initial nucleus.

The SPR experiments were performed at 6, 9, 14, 19, 23, 27, and 32 °C on a BiacoreTM T200 apparatus (GE Healthcare Life Sciences, Uppsala, Sweden) using a CM5 sensor chip (BiacoreTM) coated with 2600 resonance units (RU) of streptavidin (Roche Applied Sciences, Roche Diagnotics, Meylan France). The DNA oligonucleotides were purchased from Eurofins MWG Operon (Ebersberg, Germany). The DNA samples were prepared at 23 °C in a sodium phosphate buffer 20 m*M*, pH 7.2, NaCl 100 m*M*, supplemented with 0.050% Tween-20 (running buffer). Fifteen RU of the biotinylated polypurine strand were immobilized on one flow cell of the sensor chip. Another flow cell was left blank for double-referencing of the sensorgrams. The single cycle-kinetics method (Karlsson, Katsamba, Nordin, Pol, & Myszka, 2006) was used to inject the samples in duplicate over the target at 25 μL min^{-1}. The association and dissociation rate constants were determined by direct curve fitting of the sensorgrams according to the model $S_1 + S_2 \leftrightharpoons D$ with the Biacore T200 evaluation software V2.00.

The ITC experiments were performed in the same buffer (comprising 0.050% Tween-20) at 15, 20, 25, 30, and 35 °C with the parameters indicated in Fig. 8. The corresponding ETC curves are in Fig. 9 and the SPR curves with their fits are shown in Fig. 10. Again, the *kinITC–ETC* and SPR results are compared with Arrhenius plots (Fig. 11).

In agreement with Line 4 in Table 1, the ETCs are extremely sharp: the c values at 15 and 20 °C are 3147 and 1610, which lead to half-height widths (in stoichiometric ratio) of 0.11 and 0.16, respectively. Beyond 20 °C, the ETCs become featureless with favorable c values of 371 and 127, but large Θ values (Line 5 in Table 1) of 2.94 and 2.40, at 25 and 30 °C, respectively. There are thus opposite patterns (high c − low Θ) at 15 and 20 °C and (low c − high Θ) at 25 and 30 °C. The very high c values yield sharp ETCs, but prevent from obtaining accurate K_d values, whereas high Θ values prevent from distinguishing the kinetic signal from the instrument response time. On the basis of the Θ values, one would conclude that there is kinetic information only at 15 and 20 °C. However, one has to admit that the Arrhenius plots (Fig. 11) show that the systematic evolution of the k_{off} values from *kinITC–ETC* follows well that from SPR at 25 °C ($10^3/T = 3.35$ K^{-1}) and 30 °C ($10^3/T = 3.30$ K^{-1}). It is important to note that, for both *kinITC–ETC* and SPR, the experiments at the highest temperatures (32 °C for SPR ad 35 °C for ITC) were discarded as they did not provide kinetic information.

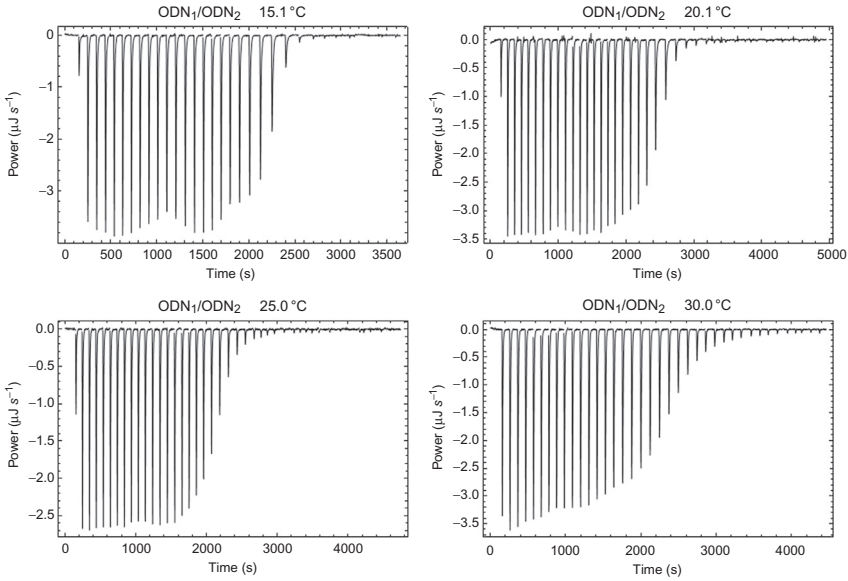

Figure 8 Example of baseline-corrected injections curves for ODN_1/ODN_2. The initial concentrations of ODN_1 (compound *A*) were $[A]_0 =$ **10** and 2.5 µ*M* at 15 °C; **10**, 2.5 and 2.5 µ*M* at 20 °C; **7.1** µ*M* at 25 °C; **10** µ*M* at 30 °C. The concentration of ODN_2 were τ_{ITC} 100 µ*M* at all temperatures and the injected volumes were **1**, 0.5, 1 µL at 15 °C; **1**, 0.5 and 0.7 µL at 20 °C; **0.7** µL at 25 °C and **1** µL at 30 °C. The underlined values in bold are those for the figures shown.

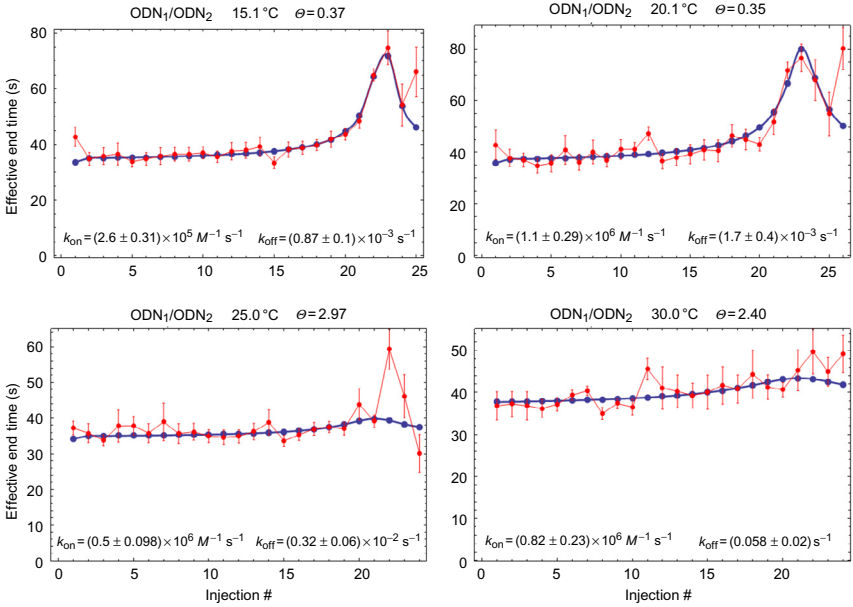

Figure 9 Fit of ODN_1/ODN_2 ETCs. Each ETC corresponds to the injection curves shown in Fig. 8. Only two injections were kept after the maximum as the effective end times were poorly determined for the following injections, which negatively affected the results. The *c* values (Wiseman parameter) are 3147, 1610, 371, and 127 from 15.1 °C to 30 °C. The parameter Θ indicated on top of each figure is defined in Table 1 and discussed in Appendix.

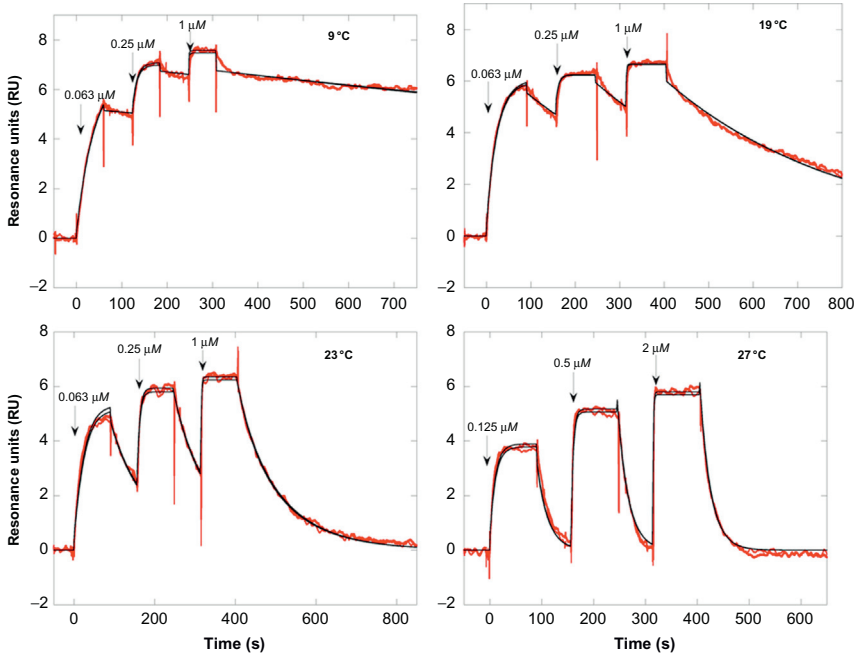

Figure 10 Kinetic analysis by SPR of duplex formation (ODN_1/ODN_2). Four experimental curves and their fits (black curves) are shown among seven. The analyte was prepared in the running buffer and injected sequentially in the order of increasing concentrations as indicated by the arrows. The regeneration of the surface was achieved with a 2-min pulse of 20 m*M* NaOH.

These results can be compared further, both on kinetic and thermodynamic grounds. First, it is striking that the activation energies of k_{on} are almost null (and even slightly negative for SPR), whereas the activation energies of k_{off} from *ITC-ETC* and SPR (Fig. 11) are large, as expected. This is in agreement with the association process not being one-step and, according to Craig et al. (1971) and Porschke and Eigen (1971), only apparent activation energies were obtained for which slightly negative values for k_{on} were indeed expected. Second, the fact that K_d values were obtained both by ITC and SPR, and that enthalpy values were obtained by ITC opens the way for a comparison of the experimental and van 't Hoff-determined enthalpy values (Fig. 12).

In both ITC and SPR, it appears that the van 't Hoff plots are significantly curved but also show distinct differences. As a consequence, the ΔH values (ΔH_{vH}) derived from the respective van 't Hoff plots are different

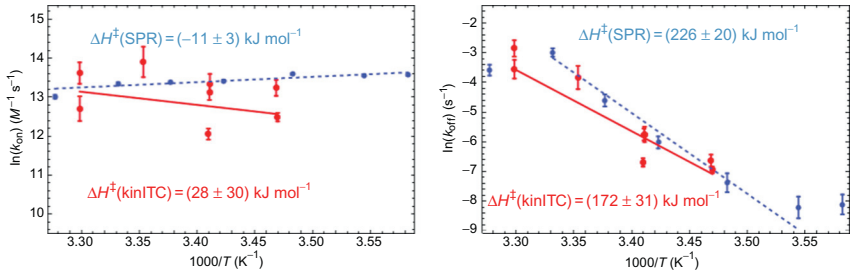

Figure 11 Arrhenius plots for the comparison of *kinITC–ETC* and SPR results for ODN_1/ODN_2. The *kinITC–ETC* results (continuous lines) are compared to the SPR results (dashed lines). The corresponding activation energies are indicated. The SPR data were not included in the Arrhenius plots at the highest (32 °C) and lowest (6 and 9 °C) temperatures due to obvious departure from linear variation for k_{off}.

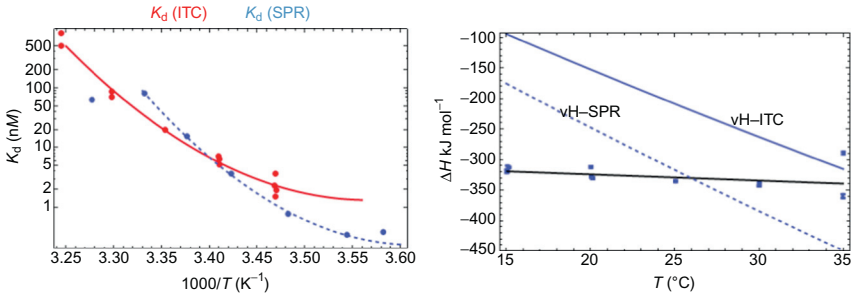

Figure 12 Comparison of van 't Hoff-derived enthalpies from ITC and SPR for ODN_1/ODN_2. Left: evolution of K_d from ITC (solid curve) and from SPR (dashed curve) versus $1/T$. The curves were obtained by a fit of the experimental K_d values (dots) with the van 't Hoff equation and a temperature-dependent ΔH according to $\Delta H = \Delta H_0 + \Delta C_p\,(T - T_0)$ and $1000/T_0 = 3.40\ K^{-1}$. Note that the end points were excluded from the fit for the SPR data. Right: comparison of the plots of $\Delta H = \Delta H_0 + \Delta C_p\,(T - T_0)$ derived from ITC and SPR van 't Hoff plots with the experimental ΔH values from ITC (solid line with squares).

(Fig. 12, right). There is another important feature: None of the ΔH_{vH} agree with ΔH_{ITC}. Even more striking, ΔH_{vH} from K_d(ITC) differs most from ΔH_{ITC}! This fact is so clear that it deserves discussion. First, recall that such differences between ΔH_{vH} and ΔH_{ITC} are not unusual (Naghibi, Tamura, & Sturtevant, 1995). The fact that association does not follow a simple one-step process (a purely kinetic feature) cannot be the cause of such a thermodynamic discrepancy. The more likely explanation is that the data do not represent merely the formation of a full duplex. The two sequences ODN_1 and

ODN_2 were designed to avoid hairpin formation but, prompted by the latter comment, one notices that two symmetric imperfect associations can form (non-WC base pairs are in bold):

```
5′-AAG AAG AGG AG-3′          5′-AAG AAG AG GAG-3′
   3′-TTC TTC TC CTC-5′       3′-TTC TTC TCC TC-5′
```

There is no reason why these two imperfect associations would not compete with full duplex formation, particularly at low temperature. Not only are there two possible competing structures but, in addition, dangling strands are known to stabilize terminal base pairs (Turner, 2000). Although a full study would be required, additional remarks will support this explanation. From the values of K_d and ΔH from ITC at each temperature T, the melting temperature T_m can be derived following:

$$\frac{1}{T_m} = \frac{1}{T} - \frac{R}{\Delta H} \mathrm{Ln} \frac{4K_d}{[\mathrm{ODN}]_{tot}} \tag{9}$$

with $R = 8.314\ \mathrm{J\ mol^{-1}\ K^{-1}}$ being the gas constant and $[\mathrm{ODN}]_{tot}$ the total strand concentration at unit stoichiometry. Equation (9) derives from $\Delta G^0 = \Delta H^0 - T\Delta S^0 = RT\mathrm{Ln}K_d$ and $T_m^0 = \Delta H^0/\Delta S^0$, where T_m^0 is the melting temperature in the standard conditions ($[\mathrm{ODN}]_{tot} = 1M$); T_m in the conditions of the experiment derives from T_m^0 by the necessary correction on concentration (the factor 4 in Eq. 9 comes from the annealing of two different strands) (Dumas, Ennifar, Disdier, & Walter, 2014; Turner, 2000). The resulting T_m values are in Fig. 13, which shows a systematic increase from 30 to 40 °C. Obviously, this melting temperature would not change with the temperature if a single species were present; the observed change is thus a strong indication of the presence of less stable species at low temperatures.

Interestingly, the theoretical T_m (Kibbe, 2007) of the imperfect association (with a G-T base pair) is either 24 or 30 °C depending on how the calculation is done, and the theoretical T_m of the full duplex is 41.9 °C, in good agreement with the maximum T_m at high temperature (Fig. 13). Also note that the ΔH_{vH} from K_d(ITC) and the measured ΔH_{ITC} are very different at low temperature but become almost equal at 35 °C (Fig. 12), which is again in agreement with a majority of the stable full duplex at that temperature.

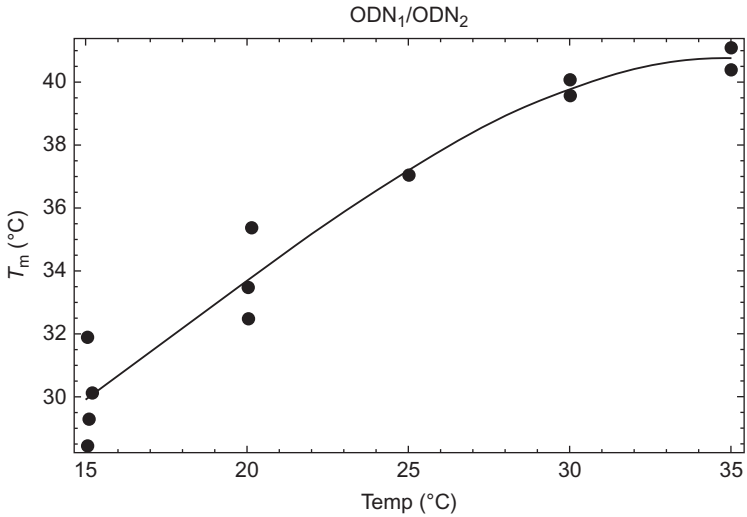

Figure 13 Evolution of the melting temperature from ITC results. The melting temperatures from Eq. (9) used with the K_d and ΔH values from all ITC experiments with ODN_1/ODN_2 are shown as dots. The curve is merely a guide for the eye.

5. INSTRUMENT RESPONSE TIME: MEASUREMENT AND IMPORTANT FACTS

Characterization of the instrument response time (for any instrument such that the response is linearly related to the excitation) is based on measuring the response to an "instantaneous" excitation, in practice to a very quick excitation. For that, one can use the dilution of a small amount of methanol into water. The differential heat of dilution of pure methanol into a large excess of water (-7.347 kJ mol^{-1}) (Bertrand, Millero, Wu, & Hepler, 1966) is too important for a modern microcalorimeter, which makes necessary to inject diluted methanol (1–2%, v/v). In view of *kinITC* experiments, the instrument must be used in the "power compensation mode," as the "heat conduction mode" would increase considerably the response time. With our ITC200 and a cell volume of 203 μL, we obtained good results with injections from 0.5 to 2 μL (at a rate of 0.5 μL s^{-1}), with a maximum sampling rate of 1 s and with a mixing speed of 1500 rpm (it may happen that 1000 rpm give better results). An estimate of the response time is obtained by an exponential fit of the end part of the power curve as shown in Fig. 14A. As a rule of thumb, one may consider as the first experimental point to be kept the one for which the power amplitude is half the maximum amplitude.

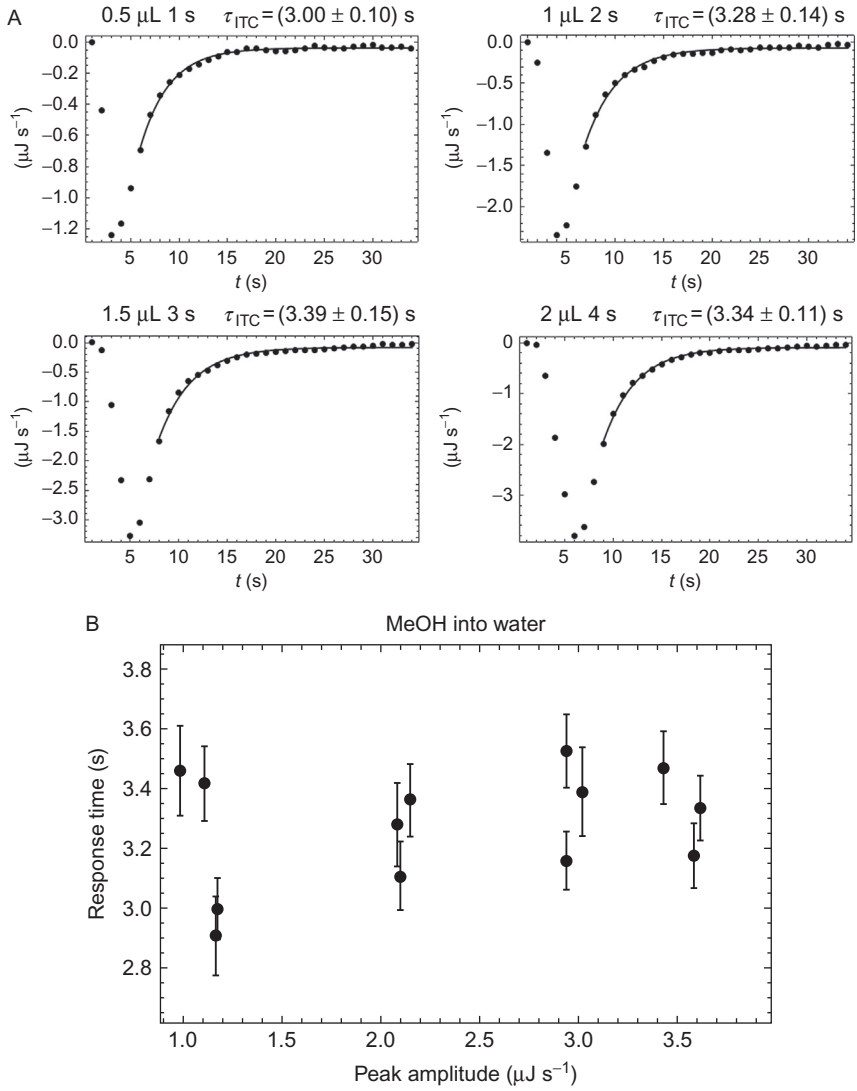

Figure 14 Response time determination. (A) Examples of data obtained with injection of methanol (1%, v/v) into water at 15 °C. The injected volumes, injection times, and response times obtained after the exponential fit (solid curves) are indicated. (B) Stability of the response times versus the amplitude of the excitation for repeated measurements.

Normally, no systematic variation of the response time with the amplitude of the signal should be seen, as in Fig. 14B. However, Fig. 14B shows significant spreading, which means that a single measurement is highly suspicious.

In addition, it should be mentioned that non-monotonous response curves with positive excursions before the return to baseline can be obtained. Such response curves should be discarded. This type of artifact results from an overshoot of the power compensation mechanism of the instrument (electronics and software), which shows that one is close to instability due to the very quick excitation following methanol dilution.

There is another fact of considerable practical importance. Contrary to a common belief, the response time is not in reality an intrinsic property of an ITC instrument since it strongly depends on the cleanness of the measurement cell. We observed, for example, that the response time obtained with the same instrument and using the same procedure (dilution of methanol) could be as high as 7 s, that is twice as much as in Fig. 14. However, there was a return to low values after extensive cleaning of the instrument with the recommended procedure. It is thus clear that frequent and quick measurement of the response time should be made. In any case, an experiment made in view of obtaining kinetic information, particularly for fast kinetics, should be preceded by such a measurement and, if necessary, by cleaning of the instrument.

6. CONCLUSIONS

The *kinITC–ETC* method, a simplified version of *kinITC* (Burnouf et al., 2012), has been examined to assess its theoretical foundation and its practical ability of obtaining kinetic information by comparison with SPR data. Apart in one case (HIV-1-RT/Nevirapine), the results from *kinITC–ETC* were noisier than those from SPR. This appeared with regression lines in Arrhenius plots being less well defined than their SPR counterparts (Figs. 5 and 11). Nevertheless, *kinITC–ETC* obtained excellent results with carbonic anhydrase/4-CBS and k_{on} and k_{off} values in the ranges 10^4–$3 \times 10^4\ M^{-1}\ s^{-1}$ and 5×10^{-3}–$3 \times 10^{-2}\ s^{-1}$. In particular, the temperature dependence was perfectly obtained. The results are reasonably good with HIV-1-RT/Nevirapine and k_{on} and k_{off} values in the ranges 10^3–$3 \times 10^3\ M^{-1}\ s^{-1}$ and 2×10^{-3}–$1.5 \times 10^{-2}\ s^{-1}$. The temperature dependence, however, was not clearly defined. It is fair to say that SPR data (at one temperature only) also showed variability with replicate experiments. The greater dispersion of the results from *kinITC–ETC* is manifest for ODN_1/ODN_2 (Fig. 11). However, the results are reasonably good at

15 and 20 °C ($k_{on} \sim (4 \pm 2) \times 10^5\ M^{-1}\ s^{-1}$ and k_{off} values in the range 10^{-3}–$3 \times 10^{-3}\ s^{-1}$) and deviate slightly from SPR results at the higher temperatures 25 and 30 °C where the kinetics is still faster ($k_{on} \sim (4 \pm 2) \times 10^5\ M^{-1}\ s^{-1}$ and k_{off} values in the range 10^{-2}–$4 \times 10^{-2}\ s^{-1}$). It is quite noticeable that the two techniques reached their limit at the same point: the SPR data were not usable at 32 °C and the ITC data were not usable at 35 °C.

Several important practical recommendations can be made. First, the instrument must be cleaned very thoroughly. Second, one should have a sufficient sampling of the ETC, which means that small stoichiometry increments are preferable as far as the heat power is high enough. Of course, in case of fast kinetics, one should try to lower the concentrations of compounds A and B as much as possible. In this respect, low ΔH values are obviously quite detrimental.

In conclusion, *kinITC–ETC* is a new mean of obtaining kinetic information, potentially in a wide range of k_{on} values, from 10^3 to $5 \times 10^5\ M^{-1}\ s^{-1}$. A great interest of *kinITC–ETC* is of not requiring any sample preparation. In addition, due to its implementation in AFFINImeter (https://www.affinimeter.com/), *kinITC–ETC* results can be obtained without requiring specific knowledge or any action from the user. We therefore anticipate that *kinITC–ETC* will become a standard tool in biology. Lastly, we think it is necessary to recall that all kinetic method are model dependent, which means that the results cannot be correct if the kinetic model is not correct.

ACKNOWLEDGMENTS

We are indebted to F. Disdier for the development and to M. Zerbib for the maintenance of the web site (http://www-ibmc.u-strasbg.fr:8080/webMathematica/kinITCdemo/).

APPENDIX. GEOMETRICAL FEATURES OF AN ETC

The analysis performed in Dumas (2015) allowed to determine all geometrical characteristics of an ETC (Fig. 15). The results, obtained by making the approximation that the injection and mixing times are negligible, are given in Table 1 with reference to Fig. 15.

The parameter Θ was obtained in Burnouf et al. (2012) as a way of quantifying the possibility of discerning the true kinetic signal from the kinetic response of the instrument. With more experience, we can now state that it is safe to have $\Theta < 0.5$. However, examples obtained with ODN_1/ODN_2 showed that significantly higher values allowed obtaining kinetic information.

Table 1 Geometrical Features of an ETC (see Fig. 15) Notations: $[A]_0$, Initial Concentration in the Cell; $c = [A]_0/K_d$ (Wiseman Parameter); τ_{ITC}, Response Time of the Instrument; s is the Current Stoichiometric Ratio $[B]_{tot}/[A]_{tot}$

1. Min. equilibration time (at $s=0$)	$\alpha\left[\frac{1}{k_{off}(c+1)}+\tau_{ITC}\right]$	Lower horizontal line ($\alpha \approx 4.5$)
2. Max. equilibration time (at $s=1-1/c$)	$\alpha\left[\frac{1}{2k_{off}c^{1/2}}+\tau_{ITC}\right]=\alpha\tau_{ITC}\left[1+\frac{1}{2\Theta}\right]$	Upper short line (Θ defined below)
3. Max. equilibration time variation:	$\alpha k_{off}^{-1}\left[\frac{1}{2c^{1/2}}-\frac{1}{c+1}\right]$	Length of the vertical arrow (at $s=1-1/c$)
4. Half-height width	$\frac{4\left(1-c^{-1/2}\right)\sqrt{3+2c^{1/2}+3c}}{\left(1+c^{1/2}\right)^2}$	Length of the half-height dashed line
5. Parameter Θ	$\sqrt{k_{off}k_{on}[A]_0}\tau_{ITC}=c^{1/2}k_{off}\tau_{ITC}$	Defined in Burnouf et al. (2012)

It is remarkable that the maximum amplitude of equilibration time variation (arrow in Fig. 15) does not depend on τ_{ITC} and the half-height width only depends on c.

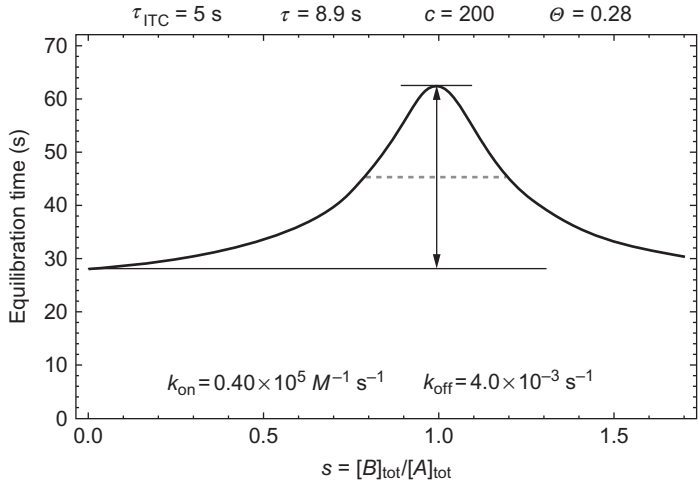

Figure 15 Geometrical features of an ETC. The minimum equilibration time at $s=0$ (lower horizontal line), the half-height width (dashed line), the maximum equilibration time (upper short line), and the maximum amplitude (vertical arrow) are highlighted. All values used to calculate the ETC are indicated. See Table 1 for equations.

REFERENCES

Bertrand, G. L., Millero, F. J., Wu, C. H., & Hepler, L. G. (1966). Thermochemical investigations of the water-ethanol and water-methanol solvent systems. I. Heats of mixing, heats of solution, and heats of ionization of water. *Journal of Physical Chemistry*, *70*, 699–705.

Burnouf, D., Ennifar, E., Guedich, S., Puffer, B., Hoffmann, G., Bec, G., et al. (2012). kinITC: A new method for obtaining joint thermodynamic and kinetic data by isothermal titration calorimetry. *Journal of the American Chemical Society*, *134*(1), 559–565.

Buzzell, A., & Sturtevant, J. M. (1951). A new calorimetric method. *Journal of the American Chemical Society*, *73*, 2454–2458.

Calvet, E., & Prat, H. (1963). *Recent progress in microcalorimetry*. Oxford: Pergamon Press.

Craig, M. E., Crothers, D. M., & Doty, P. (1971). Relaxation kinetics of dimer formation by self-complementary oligonucleotides. *Journal of Molecular Biology*, *62*, 383–401.

De Clercq, E. (1998). The role of non-nucleoside reverse transcriptase inhibitors (NNRTIs) in the therapy of HIV-1 infection. *Antiviral Research*, *38*, 153–179.

Dumas, P. (2015). Joining thermodynamics and kinetics by kinITC. In M. Bastos (Ed.), *Biocalorimetry: Foundations and contemporary approaches*.Boca Raton: Taylor & Francis. in press.

Dumas, P., Ennifar, E., Disdier, F., & Walter, P. (2014). UV melting studies with RNA. In *Handbook of RNA biochemistry* (pp. 445–480). Vol. 1. Weinheim, Germany: Wiley-VCH.

Edsall, J. T., & Gutfreund, H. (1983). *Bio-thermodynamics: The study of biochemical processes at equilibrium*. New York: John Wiley & Sons.

Egawa, T., Tsuneshige, A., Suematsu, M., & Yonetani, T. (2007). Method for determination of association and dissociation rate constants of reversible bimolecular reactions by isothermal titration calorimeters. *Analytical Chemistry*, *79*, 2972–2978.

Garcia-Fuentes, L., Baron, C., & Mayorga, O. L. (1998). Influence of dynamic power compensation in an isothermal titration microcalorimeter. *Analytical Chemistry*, *70*, 4615–4623.

Hansen, C. W., Hansen, L. D., Nicholson, A. D., Chilton, M. C., Thomas, N., Clark, J., et al. (2010). Correction for instrument time constant and baseline in determination of reaction kinetics. *International Journal of Chemical Kinetics*, *43*, 53–61.

Johnson, R. E., & Biltonen, R. L. (1975). Determination of reaction rate parameters by flow microcalorimetry. *Journal of the American Chemical Society*, *97*, 2349–2355.

Karlsson, R., Katsamba, P. S., Nordin, H., Pol, E., & Myszka, D. G. (2006). Analyzing a kinetic titration series using affinity biosensors. *Analytical Biochemistry*, *349*, 136–147.

Kibbe, W. A. (2007). OligoCalc: An online oligonucleotide properties calculator. *Nucleic Acids Research*, *35*(Web Server issue), W43–W46.

Langerman, N., & Biltonen, R. L. (1979). Microcalorimeters for biological chemistry: Applications, instrumentation and experimental design. *Methods in Enzymology*, *61*, 261–286.

Lopez-Mayorga, O., Mateo, P. L., & Cortijo, M. (1987). The use of different input signals for dynamic characterisation in isothermal microcalorimetry. *Journal of Physics E: Scientific Instruments*, *20*, 265–269.

Naghibi, H., Tamura, A., & Sturtevant, J. M. (1995). Significant discrepancies between van't Hoff and calorimetric enthalpies. *Proceedings of the National Academy of Sciences of the United States of America*, *92*, 5597–5599.

Navratilova, I., Papalia, G. A., Rich, R. L., Bedinger, D., Brophy, S., Condon, B., et al. (2007). Thermodynamic benchmark study using Biacore technology. *Analytical Biochemistry*, *364*, 67–77.

Porschke, D., & Eigen, M. (1971). Co-operative non-enzymic base recognition. 3. Kinetics of the helix-coil transition of the oligoribouridylic–oligoriboadenylic acid system and of oligoriboadenylic acid alone at acidic pH. *Journal of Molecular Biology*, *62*, 361–381.

Privalov, P. L. (1979). Stability of proteins: Small globular proteins. *Advances in Protein Chemistry*, *33*, 167–241.
Ren, J., Esnouf, R., Garman, E., Somers, D., Ross, C., Kirby, I., et al. (1995). High resolution structures of HIV-1 RT from four RT-inhibitor complexes. *Nature Structural Biology*, *2*, 293–302.
Tachoire, H., Macqueron, J. L., & Torra, V. (1986). Traitement du signal en microcalorimétrie: Applications en cinétique et thermodynamique. *Thermochimica Acta*, *105*, 333–367.
Tian, A., & Cotie, J. (1924). Utilisation en biologie de la méthode microcalorimétrique; exemple d'application. *C.R.A.S. (Paris)*, *178*, 1390–1392.
Turner, D. H. (2000). Conformational changes. In V. A. Bloomfield, D. M. Crothers, & I. Tinocco (Eds.), *Nucleic acids, structure, properties and functions* (pp. 259–334). Sausalito, CA: University Science Books.
Vander Meulen, K. A., & Butcher, S. E. (2012). Characterization of the kinetic and thermodynamic landscape of RNA folding using a novel application of isothermal titration calorimetry. *Nucleic Acids Research*, *40*, 2140–2151.
Vander Meulen, K. A., Horowitz, S., Trievel, R. C., & Butcher, S. E. (2015). Measuring the kinetics of molecular association by isothermal titration calorimetry. In A. Feig (Ed.), *Calorimetry* (pp. 179–212). Oxford: Elsevier.
Watt, G. D., & Sturtevant, J. M. (1969). The enthalpy change accompanying the oxidation of ferrocytochrome c in the pH range 6–11 at 25 degrees. *Biochemistry*, *8*, 4567–4571.
Willson, R. J., Beezer, A. E., Mitchell, J. C., & Loh, W. (1995). Determination of thermodynamic and kinetic parameters from isothermal heat conduction microcalorimetrey: Application to long-term-reaction studies. *Journal of Physical Chemistry*, *99*, 7108–7113.
Wiseman, T., Williston, S., Brandts, J. F., & Lin, L. N. (1989). Rapid measurement of binding constants and heats of binding using a new titration calorimeter. *Analytical Biochemistry*, *179*, 131–137.